Geophysical Journal International

Geophys. J. Int. (2012) **190,** 179–187 doi: 10.1111/j.1365-246X.2012.05516.x

Modelling petroleum migration through microcrack propagation in transversely isotropic source rocks

Z. Q. Fan,[1] Z.-H. Jin[1] and S. E. Johnson[2]

[1]*Department of Mechanical Engineering, University of Maine, Orono, ME* 04469*, USA. E-mail: zhihe.jin@maine.edu*
[2]*Department of Earth Sciences, University of Maine, Orono, ME* 04469*, USA*

Accepted 2012 April 19. Received 2012 April 17; in original form 2011 November 18

SUMMARY

To investigate primary petroleum migration through microfracturing of source rocks, we develop a theoretical multiphysics model incorporating simultaneous generation of oil and gas from kerogen, elastic anisotropy of the source rock and propagation of microcracks filled with oil and gas. The variations of excess fluid pressure in the crack and crack propagation distance with time are determined. A detailed parametric analysis is performed to study the sensitivity of petroleum migration behaviour to changes in the input parameters including kerogen type (chemistry of kerogen to oil/gas conversion), elastic anisotropy of source rocks, geothermal gradient and burial rate. Numerical results show that a microcrack in type III kerogen-bearing source rocks can attain greater length than in rocks containing type I and II kerogen which have higher oil potentials and transform to oil/gas much faster than type III kerogen. Elastic anisotropy of source rocks has a profound influence on the crack propagation distance, but only a marginal effect on the duration of crack propagation and the excess fluid pressure. The simulation also shows that higher geothermal gradients and fast burial reduce the crack propagation duration significantly, but excess pressure and final crack length are not sensitive to the variations of geothermal gradient and burial rate.

Key words: Numerical approximations and analysis; Geomechanics; Elasticity and anelasticity; Equations of state; Fracture and flow; Mechanics, theory, and modelling.

1 INTRODUCTION

Petroleum forms in fine-grained source rocks and accumulates in coarse-grained reservoir rocks with relatively higher porosity and permeability. The release of petroleum within source rocks and subsequent expulsion to the more permeable carrier and reservoir rocks is called primary petroleum migration (Tissot & Welte 1984). Although great advances have been made in the understanding of primary migration, quantitative models are still lacking that characterize the petroleum migration route and distance. An improved understanding of petroleum migration through quantitative modelling would help in the exploration of petroleum as modelling results can be applied to the selection of favourable exploration zones based on the available geological data.

Petroleum migration and generation are interrelated and inseparable (Momper 1978). Sedimentary rocks rich in organic materials are subjected to continuous burial due to a number of geological processes, for example, lithospheric flexure associated with orogeny and compaction. As burial proceeds, organic materials undergo successive evolution in response to the temperature and pressure changes caused by the progressive subsidence. Under specific temperature and pressure conditions kerogen forms from the organic materials deposited and preserved in the sediments. With increasing depth of burial, temperature and pressure continue to increase. When kerogen becomes 'mature', it begins to release liquid oil. Depending on the type of kerogen, significant amount of gas can form simultaneously with liquid oil (Tissot & Welte 1984). Based on the chemical composition, active kerogen is typically classified into three types. Type I is mainly formed from lipids and has higher potential for liquid oil. Type II comes principally from marine organic matter and tends to produce a mix of oil and gas. Its oil potential is lower than that for type I but higher than that for type III that is usually derived from terrestrial higher plant. Type II kerogen is the most common in sedimentary rocks (Hunt 1979; Tissot & Welte 1984; Luo & Vasseur 1996).

The increasing overburden load during continuous burial of the sedimentary rocks leads to an increase in bulk density and loss of porosity and permeability. Pore size and permeability become smaller with increasing depth, which renders porous flow through the dense source rock matrix highly ineffective (Tissot & Welte 1984; Mann 1994). Petroleum migration through microfracturing of the source rocks caused mainly by oil/gas generation is cited as an effective mechanism for primary migration at great depths (e.g. Durand 1988; Hunt 1990; Capuano 1993; Vernik 1994; Marquez & Mountjoy 1996; Nelson 2001; Lash & Engelder 2005; Jin *et al*. 2010).

The conversion of kerogen to oil and gas results in appreciable volume increase due to the density difference between the precursor and the products. As a result, overpressure is developed within the source rocks. Furthermore, parallel to the kerogen transformation, part of the overburden load is transferred from the solid source rock matrix to the enclosed petroleum mix, which expedites the overpressure build-up process. Clay-size minerals within the source rocks act as effective seals, which prevent the pressure caused by petroleum generation from dissipating. When the overpressure reaches a critical value, microcracks will initiate and propagate thus creating a pathway for migration of petroleum (Momper 1978; Durand 1988). As the transformation goes forward, further growth of microcracks driven by the excess pressure enables the migration to proceed. The preferential direction of initial migration is parallel to the bedding surfaces for the following reasons: (a) oil-generating kerogen particles tend to be more concentrated along the bedding surfaces and most of the particles are aligned parallel to the bedding with high aspect ratio (Lash & Engelder 2005), and (b) strength anisotropy of the source rock favours horizontal migration of petroleum, that is, fracture toughness of the source rocks along the bedding is generally lower than that in the direction perpendicular to the bedding (Momper 1978; Vernik 1994; Lash & Engelder 2005) and, hence, microcracks filled by oil and/or gas tend to grow in the bedding plane. Microcracks propagating along the bedding surfaces may coalesce and reach pre-existing vertical fractures, thus, forming an interconnected fracture network and facilitating further migration of petroleum (Momper 1978; Vernik 1994; Fan *et al*. 2010).

Many attempts have been made to correlate petroleum migration with the microfracturing of source rocks, including theoretical modelling and characterization, experimental simulation and field observation (Ozkaya 1988; Engelder & Lacazette 1990; Lacazette & Engelder 1992; Miller 1995; Nunn 1996; Law & Spencer 1998; Jin & Johnson 2008; Fan *et al*. 2010). Momper (1978) presented an extensive review on petroleum migration within the source rocks concerning organic geochemistry, petrophysics and petroleum geology. Palciauskas & Domenico (1980) considered the microfracture initiation associated with hydrocarbon generation and sediment compaction. Field observations from different locations given by Comber & Hinch (1987) and Marquez & Mountjoy (1996) lend support to the idea that microfractures are efficient migration routes for oil in relatively impermeable rocks. Bredehoeft *et al*. (1994) examined the role of overpressure in driving fluid movement and simulated the microcrack initiation as a result of kerogen conversion to oil. Berg & Gangi (1999) estimated the overpressure resulting from oil generation and analysed the microfracturing of compacted, relatively impermeable source rocks using the Coulomb criterion without considering crack propagation. Based on laboratory test, Vernik (1994) suggested that microfracturing is a natural consequence of kerogen transformation to oil due to the strong strength anisotropy and the favourable kerogen particle orientation within the dense source rocks. Convincing evidence supporting petroleum migration through microcrack growth is provided by Lash & Engelder (2005). They found bitumen-filled microcracks showing the characteristics of decomposition of kerogen to oil during catagenesis. Jin *et al*. (2010) developed a model of primary oil migration by collinear microcrack coalescing during the main stage of oil generation. Their results indicated that microcracks would propagate subcritically because excess pressure induced by kerogen transformation to petroleum is not high enough to drive critical crack growth. Fan *et al*. (2010) considered the subcritical growth of a penny-shaped crack driven by excess pressure caused by oil generation in an isotropic source rock matrix.

The source rocks have been assumed as an isotropic solid in the existing models of primary migration through fracture propagation. However, a typical source rock has a laminated structure with organic-rich layers alternating with organic-poor layers. Such a structure gives rise to a strong elastic anisotropy. Moreover, the interlayer strength is weaker than the in-plane strength (Vernik 1994; Vernik & Landis 1996). The existing modelling investigations only considered generation of single-phase petroleum (oil or gas) during crack propagation. However, kerogen is converted to oil and gas simultaneously under most pressure and temperature conditions. Hence, source rock anisotropy and simultaneous generation of oil and gas must be considered to better understand the process of petroleum migration.

In this paper, we extend our previous work (Fan *et al*. 2010, 2012) to the more general case where elastic anisotropy and simultaneous kerogen to oil/gas transformation are taken into account. We analyse the subcritical growth of a penny-shaped crack fully filled by oil and gas driven by the overpressure induced by the conversion of kerogen to the petroleum mix. The conversion of oil to gas is not considered. A sensitivity analysis is carried out to study the effects of various parameters on the petroleum migration behaviour, including kerogen type, material anisotropy, geothermal gradient and burial rate. Detailed results are given for the overpressure evolution with time and microcrack propagation distance.

2 THEORETICAL MODELLING OF PRIMARY PETROLEUM MIGRATION THROUGH SUBCRITICAL CRACK PROPAGATION DURING HYDROCARBON GENERATION

2.1 Kerogen transformation kinetics

According to Tissot & Welte (1984) and Berg & Gangi (1999), the transformation of kerogen to hydrocarbons obeys the following first-order kinetics equation:

$$\frac{\mathrm{d}M}{\mathrm{d}t} = -BM\exp\left[-\frac{E_{\mathrm{A}}}{RT(t)}\right], \tag{1}$$

where M is the mass of active kerogen at time t, B is the frequency factor, E_{A} is the activation energy of the transformation, R is the universal gas constant and T is the absolute temperature. The temperature T of a kerogen particle under transformation varies with time t through the geothermal gradient G and burial rate S. In this study, we assume a constant burial rate and a constant geothermal gradient, which are reasonable for the principal zone of petroleum generation in the depth range of 3–6 km.

Similar to the oil/gas conversion case (Fan *et al*. 2012), we obtain the kerogen mass at time t by integrating eq. (1) and considering burial rate and geothermal gradient as follows:

$$M = M_0\exp\left[-\Phi(t)\right], \tag{2}$$

where M_0 is the initial mass of kerogen particle and $\Phi(t)$ is given by

$$\Phi(t) = \frac{B(T_0+GSt)}{GS}\exp\left[-\frac{E_A}{R(T_0+GSt)}\right] - \frac{BT_0}{GS} \times \exp\left(-\frac{E_{\mathrm{A}}}{RT_0}\right) + \frac{BE_{\mathrm{A}}}{RGS}\left\{E_i\left[-\frac{E_{\mathrm{A}}}{R(T_0+GSt)}\right] - E_i\left(-\frac{E_{\mathrm{A}}}{RT_0}\right)\right\}, \tag{3}$$

in which $E_i()$ is the exponential integral defined by

$$E_i(x) = \int_{-\infty}^{x} \frac{e^{x'}}{x'} dx'.$$

Accompanying the oil generation during the successive evolution of kerogen, some amount of gas is released of which methane accounts for the major constituent. Neglecting the mutual solubility of gas and oil, we can get the volumes of oil and gas at time t as follows:

$$V_{\text{oil}} = \frac{fM_0}{\rho_{\text{oil}}} \{1 - \exp[-\Phi(t)]\}, \tag{4}$$

$$V_{\text{gas}} = \frac{(1-f)M_0}{\rho_{\text{gas}}} \{1 - \exp[-\Phi(t)]\}, \tag{5}$$

where ρ_{oil} and ρ_{gas} are the densities of oil and gas, respectively, and f is the mass fraction of oil in the generated petroleum compound.

2.2 Equation of state for gas

To describe the behaviour of gas under high pressures and temperatures, we must employ an appropriate equation of state. We adopt the equation of state for methane developed by Duan *et al*. (1992) which covers a wide range of temperature and pressure (0–1000 °C and 0–800 MPa, respectively). The equation of state has the following form:

$$\frac{P_r V_r}{T_r} = 1 + \frac{C_1}{V_r} + \frac{C_2}{V_r^2} + \frac{C_3}{V_r^4} + \frac{C_4}{V_r^5} + \frac{C_5}{V_r^2} \times \left(\beta + \frac{\gamma}{V_r^2}\right) \exp\left(-\frac{\gamma}{V_r^2}\right), \tag{6}$$

where

$$P_r = \frac{P}{P_c}, \quad T_r = \frac{T}{T_c}, \quad V_r = \frac{V}{V_c}, \quad V_c = \frac{RT_c}{P_c},$$

$$C_1 = a_1 + \frac{a_2}{T_r^2} + \frac{a_3}{T_r^3}, \quad C_2 = a_4 + \frac{a_5}{T_r^2} + \frac{a_6}{T_r^3},$$

$$C_3 = a_7 + \frac{a_8}{T_r^2} + \frac{a_9}{T_r^3}, \quad C_4 = a_{10} + \frac{a_{11}}{T_r^2} + \frac{a_{12}}{T_r^3} \quad \text{and} \quad C_5 = \frac{\alpha}{T_r^3},$$

in which P and T are the absolute pressure and temperature of the gas, respectively, T_c is the critical temperature above which methane cannot be liquefied regardless of the pressure applied, P_c is the critical pressure required to liquefy methane at the critical temperature T_c and $V = m/\rho_{\text{gas}}$ is the molar volume with m denoting the molar mass of methane. The above equation of state contains fifteen material parameters, a_i ($i = 1, 2, \ldots, 12$), α, β and γ, which can be found in Duan *et al*. (1992).

With the help of eq. (6), we can express the gas pressure in terms of gas density as follows:

$$P = P(\rho_{\text{gas}}) = \frac{P_c T_r V_c \rho_{\text{gas}}}{m} \left[1 + \frac{B V_c \rho_{\text{gas}}}{m} + \frac{C V_c^2 \rho_{\text{gas}}^2}{m^2} + \frac{D V_c^4 \rho_{\text{gas}}^4}{m^4} + \frac{E V_c^5 \rho_{\text{gas}}^5}{m^5} + \frac{F V_c^2 \rho_{\text{gas}}^2}{m^2} \left(\beta + \frac{\gamma V_c^2 \rho_{\text{gas}}^2}{m^2}\right) \exp\left(-\frac{\gamma V_c^2 \rho_{\text{gas}}^2}{m^2}\right)\right]. \tag{7}$$

Solving eq. (7), we can determine the density of methane gas as a function of pressure and temperature.

2.3 Material anisotropy and crack propagation model

Source rocks containing kerogen particles are anisotropic materials. The elastic moduli in the bedding plane are approximately the same. The modulus in the direction normal to bedding differs from those in the bedding plane. Hence, source rocks may be modelled as a transversely isotropic solid. The elastic properties of a transversely isotropic material can be determined by five independent elastic constants $c_{11}, c_{12}, c_{13}, c_{33}$ and c_{44} which are related to the engineering constants as follows (Lekhnitskii 1968):

$$c_{11} = \frac{E(E_z - E\nu'^2)}{(1+\nu)(E_z - E_z\nu - 2E\nu'^2)},$$

$$c_{12} = \frac{E(E_z\nu + E\nu'^2)}{(1+\nu)(E_z - E_z\nu - 2E\nu'^2)}, \quad c_{13} = \frac{E E_z \nu'}{E_z - E_z\nu - 2E\nu'^2},$$

$$c_{33} = \frac{E_z^2(1-\nu)}{E_z - E_z\nu - 2E\nu'^2} \quad \text{and} \quad c_{44} = \mu',$$

where E and ν are the Young's modulus and Poisson's ratio in the (transverse) plane of isotropy (parallel to bedding), E_z is the Young's modulus in the normal direction of the plane of isotropy and ν' and μ' are the Poisson's ratio and shear modulus between the normal and transverse directions.

Consider a subhorizontal layer-parallel kerogen particle of initial radius a_0 and thickness h undergoing transformation to generate hydrocarbons. Pressure build-up mainly caused by significant volume increase associated with the transformation overcomes the overburden pressure and initiates microfracturing. For simplicity, we assume that the microcrack with radius a_0 is formed on the kerogen surface (either on top or on bottom). As shown in Fig. 1, the microcrack is filled with oil and gas and the excess pressure on the crack surface is denoted by Δp_0 (fluid pressure beyond the overburden pressure, Engelder & Lacazette 1990). As transformation continues, a microcrack driven by the excess pressure may grow further. At time t, the crack radius is denoted by a, and the excess pressure on the crack surface Δp is determined by

$$\Delta p = P(\rho_{\text{gas}}) - \rho_s g z = P(\rho_{\text{gas}}) - \rho_s g (H_0 + St), \tag{8}$$

where ρ_s is the average sediment density, $g = 9.8$ m s^{-2} is gravitational acceleration, H_0 is the initial burial depth where the keorgen particle lies and $P(\rho_{\text{gas}})$ is the gas pressure given by eq. (7).

For a penny-shaped crack in a transversely isotropic material under uniform crack surface pressure, the volume of crack is determined to be (Tsai 1982)

$$V_{\text{crack}} = \frac{8\Delta p}{3K} a^3, \tag{9}$$

where K depends on the elastic constants through

$$K = \frac{c_{44}\left(c_{13} + \lambda_1^2 c_{33}\right)\left(c_{13} + \lambda_2^2 c_{33}\right)}{\lambda_1\lambda_2(\lambda_1 + \lambda_2)c_{33}(c_{13} + c_{44})}. \tag{10}$$

In eq. (10), λ_1 and λ_2 are two positive roots of the following equation:

$$c_{33}c_{44}\lambda^4 + \left(c_{13}^2 + 2c_{13}c_{44} - c_{11}c_{33}\right)\lambda^2 + c_{11}c_{44} = 0. \tag{11}$$

The stress intensity factor along the crack front is given by (Tsai 1982)

$$K_I = 2\Delta p\sqrt{a/\pi}. \tag{12}$$

Clearly during the pressure build-up process, stress intensity factor increases with the increasing excess pressure. When the stress intensity factor reaches the threshold value K_{Ith}, which is usually a

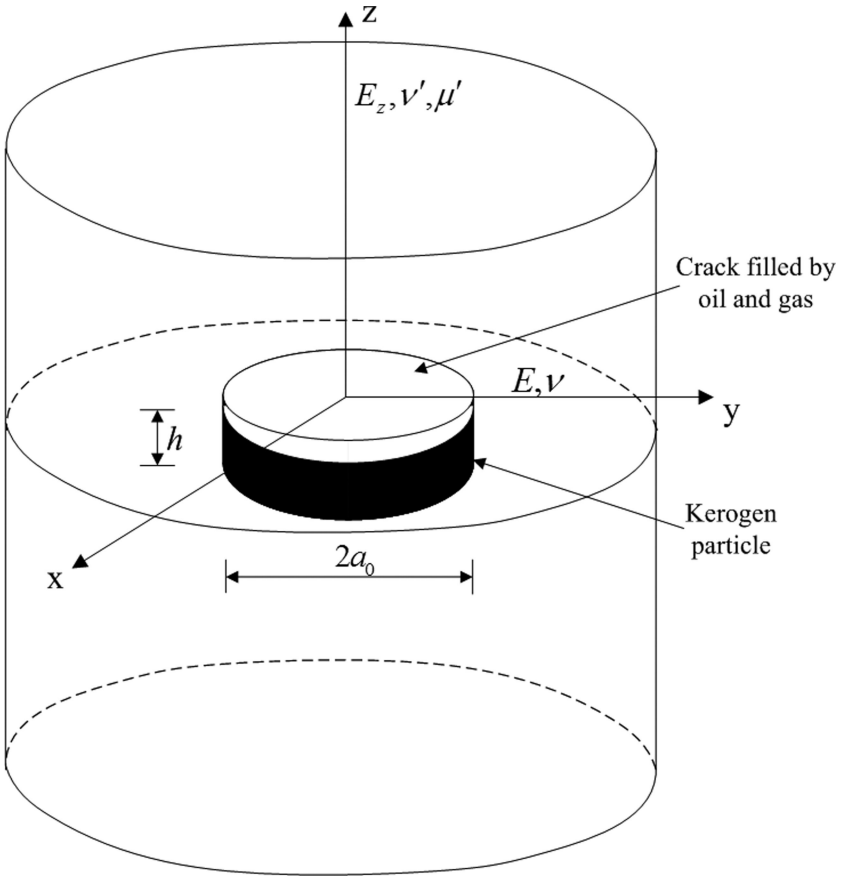

Figure 1. A penny-shaped microcrack filled by oil and gas in a transversely isotropic source rock driven by the excess pressure during kerogen–petroleum transformation.

fraction (e.g. 20–50 per cent) of the fracture toughness of the rock matrix K_{Ic}, the crack will propagate subcritically. This phenomenon is called subcritical crack propagation.

The subcritical crack propagation velocity, v, is a function of the stress intensity factor described by the Charles law (Atkinson 1984)

$$v = \frac{\mathrm{d}a}{\mathrm{d}t} = A\left[K_{\mathrm{I}}(a)\right]^n, \tag{13}$$

where n is called subcritical crack growth index and A is a material constant. Setting K_{I} in eq. (12) equal to K_{Ith}, we get the excess pressure required to initiate subcritical crack growth as follows:

$$\Delta p_{\mathrm{th}} = K_{\mathrm{Ith}}\sqrt{\pi}/(2\sqrt{a_0}). \tag{14}$$

Correspondingly the crack volume is found to be

$$V^0_{\mathrm{crack}} = \frac{8a_0^3}{3K}\Delta p_{\mathrm{th}}. \tag{15}$$

As the crack is fully saturated with oil and gas during propagation, it requires that the volume of the crack equal the sum of oil and gas volumes, that is,

$$V^t_{\mathrm{oil}} + V^t_{\mathrm{gas}} = V^t_{\mathrm{crack}}, \tag{16}$$

where V^t_{crack}, V^t_{oil} and V^t_{gas} are the volumes of the crack, oil and gas at time t, respectively. Petroleum migration does not occur until the overpressure reaches the critical value Δp_{th} after a certain amount of petroleum has already been generated. A variable of great interest is the elapsed time from the start of kerogen/petroleum conversion to the moment that the stress intensity factor reaches K_{Ith}, which is denoted by t_0. A combination of eqs (4), (5), (8), (15) and (16) gives the following two equations to determine t_0, and the corresponding gas density $\rho^{\mathrm{th}}_{\mathrm{gas}}$:

$$P\left(\rho^{\mathrm{th}}_{\mathrm{gas}}\right) - \rho_{\mathrm{s}}g(H_0 + St_0) = K_{\mathrm{Ith}}\sqrt{\pi}/\left(2\sqrt{a_0}\right), \tag{17}$$

$$\frac{(1-f)M_0\left\{1-\exp\left[-\Phi\left(t_0\right)\right]\right\}}{\rho^{\mathrm{th}}_{\mathrm{gas}}} + \frac{fM_0\left\{1-\exp\left[-\Phi\left(t_0\right)\right]\right\}}{\rho_{\mathrm{oil}}} = \frac{4a_0^3}{3K}\frac{K_{\mathrm{Ith}}\sqrt{\pi}}{\sqrt{a_0}}. \tag{18}$$

2.4 Simulation of subcritical crack growth using a finite difference approach

A finite difference method is employed to simulate the coupled process of microcrack propagation and the conversion of kerogen to oil and gas. Here, we present a brief overview of the approach (Fan *et al*. 2010). Consider subcritical propagation of a penny-shaped microcrack with an initial crack radius a_0 from time t_0 to the current time t. We need to determine the crack radius and excess pressure at time t. We apply a discretization by dividing the time domain $t - t_0$ into a uniform grid $t_0, t_1, \ldots, t_{N-1}, t_N$ with $t_N = t$. Let a_{i} and ρ^i_{gas} denote the radius of the crack and the corresponding gas density at step t_i, respectively. The crack radius at t_{i+1} is obtained

from eq. (13)

$$a_{i+1} = a_i + A[P(\rho^i_{\rm gas}) - \rho_{\rm s} g\,(H_0 + St_i)]^n (a_i)^{n/2} \left(2/\sqrt{\pi}\right)^n (t_{i+1} - t_i). \quad (19)$$

If we ignore the compressibility of oil, the gas pressure $P(\rho^{i+1}_{\rm gas})$ at t_{i+1} can be written as

$$P\left(\rho^{i+1}_{\rm gas}\right) = \frac{3K}{8a^3_{i+1}}\left[\frac{fM_0}{\rho_{\rm oil}} + \frac{(1-f)M_0}{\rho^{i+1}_{\rm gas}}\right] \times \{1 - \exp[-\Phi(t_{i+1})]\} + \rho_{\rm s} g\,(H_0 + St_{i+1})\,. \quad (20)$$

From eq. (20) $\rho^{i+1}_{\rm gas}$, the gas density at step t_{i+1}, can be solved. Correspondingly, the excess pressure Δp_{i+1} at t_{i+1} is

$$\Delta p_{i+1} = \frac{3K}{8a^3_{i+1}}\left[\frac{fM_0}{\rho_{\rm oil}} + \frac{(1-f)M_0}{\rho^{i+1}_{\rm gas}}\right]\{1 - \exp[-\Phi(t_{i+1})]\}\,. \quad (21)$$

To drive the crack propagation subcritically, Δp_{i+1} must satisfy the following condition so that the stress intensity factor at the crack front exceeds the threshold value $K_{\rm Ith}$

$$\Delta p_{i+1} \geq \frac{K_{\rm Ith}}{2\sqrt{a_{i+1}/\pi}} \quad (22)$$

If the above condition is not satisfied, which means that insufficient amount of petroleum has been released from the kerogen particle to drive subcritical crack propagation, then time t_{i+1} should be adjusted by solving eqs (17) and (18) with a_0, t_0 and $\rho^{\rm th}_{\rm gas}$ replaced by a_{i+1}, t_{i+1} and $\rho^{i+1}_{\rm gas}$, respectively. The simulation results are presented in the next section.

3 NUMERICAL RESULTS

In the numerical simulations, we focus on the effects of kerogen type (chemistry of kerogen–oil/gas conversion) and elastic anisotropy of the source rock on the crack propagation/petroleum migration behaviour. Geothermal gradient and burial rate are also considered in the simulation. Two quantities are of great interest: excess fluid pressure in the crack and crack propagation distance. The excess pressure drives crack propagation and, hence, petroleum migration. Therefore, quantitative estimation of excess pressure is crucial in the modelling of petroleum migration. Crack propagation distance is a major concern because microcrack propagation increases the possibility of forming interconnected networks that may facilitate escape of petroleum from low-permeability source rocks to higher-permeability carrier rocks. In addition, our calculations should be able to account for variations in the migration distances observed in field-based studies. The major effective source rocks seem to be fine-grained, dense, relatively impermeable argillaceous rocks, including shales, marls and argillaceous carbonates. In our simulation, we take shales as the example, and the basic material and geometrical parameters for typical shales used in the calculations are listed in Table 1 (see for example, Luo & Vasseur 1996; Nunn 1996; Berg & Gangi 1999; Lash & Engelder 2005). In particular, the fracture toughness in the bedding plane is assumed as $K_{\rm Ic} = 0.1$ MPa-m$^{1/2}$ which is consistent with the estimates of Nunn (1996) in the range of 0.01–1 MPa-m$^{1/2}$. The threshold stress intensity factor is a fraction of the fracture toughness (Atkinson 1984; Freiman 1984). We assume that $K_{\rm Ith} = 0.2\,K_{\rm Ic} = 0.02$ MPa-m$^{1/2}$.

Following Atkinson (1984), the subcritical crack growth parameters A and n are selected as $A = 8.3 \times 10^8$ mm/s/(MPa-mm$^{1/2}$)$^{\rm n}$ and $n = 80$ which yield a subcritical crack velocity of 10^{-7} mm s^{-1} when the stress intensity factor assumes the selected value of

Table 1. Physical and geometrical parameters used in the simulation.

Symbols	Definition	Value (unit)
Rock matrix		
E	In plane Young's modulus	4.0 GPa
ν	In plane Poison's ratio	0.3
E_z	Young's modulus along z direction	3.0 GPa
ν'	Poisson's ratio normal to xy plane	0.3
μ'	Shear modulus normal to xy plane	1.54 GPa
$\rho_{\rm s}$	Average sediment density	2350 kg m^{-3}
$K_{\rm Ith}$	Threshold stress intensity factor in bedding plane	0.02 MPa-m$^{1/2}$
A	Subcritical crack growth constant	8.3×10^8 mm/s/(MPa-mm$^{1/2}$)^{80}
n	Subcritical crack growth index	80
a_0	Initial microcrack radius	50 μm
H_0	Initial depth of burial	3000 m
T_0	Initial temperature	120 °C
G	Geothermal gradient	30 °C km^{-1}
S	Burial rate	0.1 km Myr^{-1}
Oil		
$\rho_{\rm oil}$	Oil density	850 kg m^{-3}
Methane		
m	Molar mass	16 g mol^{-1}
$T_{\rm c}$	Critical temperature	191.1 K
$P_{\rm c}$	Critical pressure	4.64 MPa
Kerogen		
h	Initial kerogen particle thickness	5 μm
Kinetics		
R	Universal gas constant	8.314 J/mole/K

Table 2. Kinetic parameters for three types of active kerogen.

Kerogen types	Type I	Type II	Type III
B (Pre-exponential constant)	2.44×10^{14} s^{-1}	8.14×10^{13} s^{-1}	4.97×10^{14} s^{-1}
E_A (Activation energy)	221.4 kJ mol^{-1}	215.2 kJ mol^{-1}	228.2 kJ mol^{-1}
f (Mass fraction of oil in the released compound)	86.8 per cent	82.1 per cent	60 per cent

$K_{Ith} = 0.02$ MPa-m$^{1/2}$. We note that subcritical crack growth behaviour may not be described by the Charles law over the entire stress intensity factor range from K_{Ith} to K_{Ic} (Atkinson 1984). Eq. (13) now may only be applied when the stress intensity factor is near the threshold value K_{Ith}. Our previous studies on subcritical growth of oil (or gas)-filled cracks during kerogen/oil (or oil/gas) conversion (Fan *et al*. 2010, 2012) indicated that the crack growth rate is governed by the transformation kinetics because the kerogen/oil and oil/gas conversion rates are much slower than the subcritical crack propagation rate according to the Charles law (Eq. 13). As a result, only K_{Ith} and the subcritical crack growth velocity at $K_I = K_{Ith}$ play a role in determining the crack propagation rate and duration (the crack will not grow if the stress intensity factor is smaller than K_{Ith}). Hence, Eq. (13) and the selected parameters A and n can be used to correctly describe the subcritical growth behaviour of oil/gas filled microcracks.

As described in Section 2.3, we assume that the initial crack forms on the surface of the flat kerogen particle and has the same size as that of the particle as shown in Fig. 1. Based on the field observation of Lash & Engelder (2005), we assume that the diameter and thickness of the kerogen particle are 100 and 5 μm, respectively, that is, the initial crack has a diameter of 100 μm.

We consider all three types of kerogen in the simulation. Table 2 lists the kinetic parameters for the conversion of kerogen to oil/gas (Pepper & Corvi 1995; Luo & Vasseur 1996). To explore the effect of elastic anisotropy on the crack propagation in a transversely isotropic source rock, we take the ratio of the out-of-plane Young's modus over in-plane Young's modulus, E_z/E, as an indicator of anisotropy. The material behaviour generally reduces or become similar to that of an isotropic solid when $E_z/E = 1$. For horizontal crack propagation, the fracture toughness in the vertical direction may not play an explicit role and only the toughness for crack propagation in the bedding plane is needed.

Fan *et al*. (2012) showed that steeper geothermal gradients and higher burial rates shorten the crack propagation duration but have insignificant effects on the crack propagation distance when oil converts to gas during continuous burial of oil. Here, we further examine the effects of geothermal gradient and burial rate during the conversion of kerogen to oil/gas (solid to fluids conversion instead of liquid to gas conversion). Geothermal gradient in sedimentary rocks typically ranges from 15 to 50 °C km^{-1} with an average of 30 °C km^{-1}. In our numerical calculations the basic parameters for the geothermal gradient and burial rate are taken as 30 °C km^{-1} and 0.1 km Myr^{-1}, respectively. We vary the geothermal gradient from 20 to 40 °C km^{-1} and burial rate from 0.05 to 0.2 km Myr^{-1}, consistent with previous studies (Berg & Gangi 1999).

3.1 Effect of kerogen type

We first examine the effect of kerogen type on the crack propagation distance and excess pressure for $E_z/E = 0.75$, as shown in Figs 2 and 3, respectively. It is observed from Fig. 2 that crack growth rate is the highest in type II kerogen bearing source rock and the lowest in type III kerogen bearing rock under otherwise the same conditions. The reasons lie in (1) the crack propagation rate is governed by the transformation kinetics as subcritical crack growth rate by other mechanisms is much higher than the transformation rate and (2) the higher activation energy of transformation associated with decomposition of type III kerogen leads to longer time for petroleum generation and, hence, lower subcritical crack propagation rate.

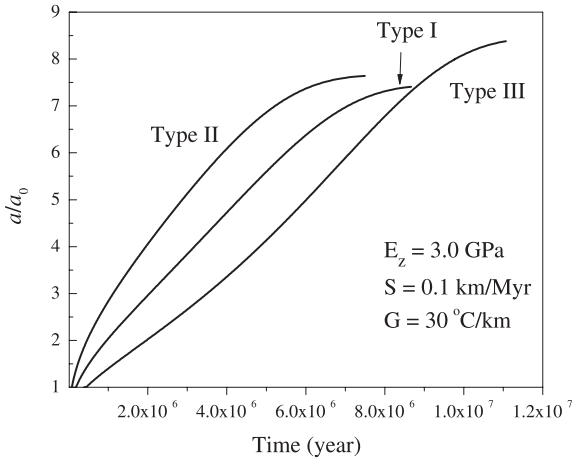

Figure 2. Normalized crack propagation distance versus time for different types of keorgen-bearing source rocks ($E_z = 3.0$ GPa, $S = 0.1$ km Myr^{-1}, $G = 30$ °C km^{-1}).

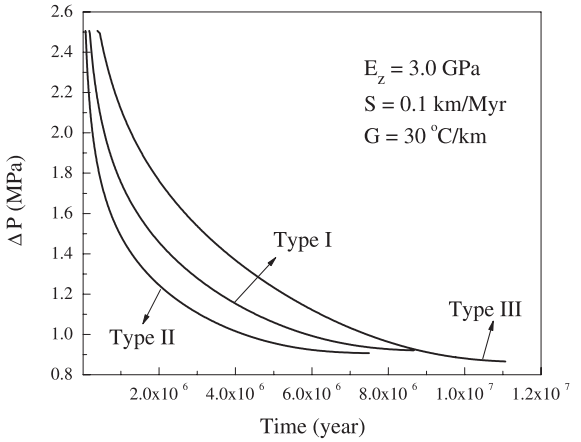

Figure 3. Excess fluid pressure versus time for different types of keorgen-bearing source rocks ($E_z = 3.0$ GPa, $S = 0.1$ km Myr^{-1}, $G = 30$ °C km^{-1}).

The final length of the microcrack in type III kerogen bearing rock is longer than those in type I and II kerogen-bearing source rocks. The reason is that relatively more gas and less oil are generated from type III kerogen. Transformation of kerogen to gas would contribute more to the volume increase due to the density difference between the precursor and the products.

Another feature of interest is the contrast between the final depths of burial for different types of kerogen when all the kerogen

transforms to petroleum. Using a simple calculation from eq. (8), we find that the final depths of burial are about 4111 and 3749 m for type III and II kerogen-bearing source rocks, respectively. The results indicate that type III kerogen is more likely to undergo secondary cracking because gas may be formed from the previously generated oil when the gas stage is reached at higher temperatures. This effect is not considered in this study.

Because longer cracks require smaller overpressure to propagate (eq. 22) excess pressure decreases with time as microcrack propagation proceeds as confirmed in Fig. 3. Although it decreases more sharply in type II and I kerogen-bearing mature source rocks, the excess pressure within the crack at the end of crack propagation is slightly different in different types of kerogen-bearing source rocks. Similar to the results from Fan *et al*. (2010), duration of crack propagation is mainly governed by the transformation kinetics because subcritical crack growth rate is higher than the transformation rate.

Type II kerogen occurs most frequently in source rocks, so in the following discussions we focus on type II kerogen for illustration purposes.

3.2 Effect of elastic anisotropy of source rocks

To investigate the sensitivity of crack propagation distance and excess pressure to elastic anisotropy of source rocks, different values of the modulus ratio E_z/E as indicators of degree of anisotropy are employed in the analysis, and the results are presented in Figs 4 and 5. The general trends of the microcrack propagation distance and excess pressure evolution through time are similar to those observed in Figs 2 and 3, respectively. The crack propagation distance increases with decreasing ratio E_z/E. At a given time, the excess pressure within the crack is lower in a source rock with a higher ratio of E_z/E. This phenomenon may be explained by observing the crack volume in eq. (9). In general, numerical calculations show that parameter K increases monotonically with increasing ratio of E_z/E, the degree of elastic anisotropy. Eq. (9) indicates that a higher K (higher E_z/E) results in a smaller crack volume for a given crack radius. Hence, the crack propagation distance becomes longer in a source rock with a higher ratio of E_z/E for a given amount of generated petroleum. Fig. 5 shows that the excess pressure decreases slightly with increasing modulus ratio E_z/E. It is interesting to note that

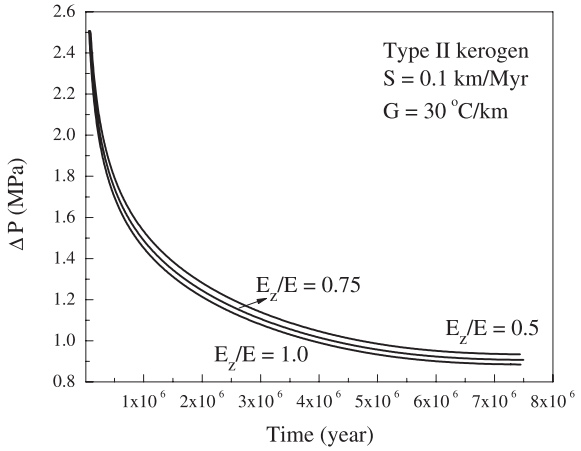

Figure 5. Effect of elastic anisotropy on the excess fluid pressure in type II kerogen-bearing source rocks ($S = 0.1$ km Myr^{-1}, $G = 30$ °C km^{-1}).

dependence of crack propagation duration on elastic anisotropy is weak and the crack propagation duration remains almost the same.

3.3 Effects of geothermal gradient and burial rate

The crack propagation distance and excess pressure profiles corresponding to three different geothermal gradients of $G = 20$, 30 and 40 °C km^{-1} are shown in Figs 6 and 7, respectively. Crack propagation duration becomes shorter at higher geothermal gradients. Correspondingly, petroleum generation and migration take place over a narrower depth range under higher geothermal gradients. For example, Fig. 6 shows that as the geothermal gradient decreases from 40 to 20 °C km^{-1}, the duration of crack propagation increases from about 6.1– 9.92 Myr. For $G = 40$ °C km^{-1}, the crack propagation starts at a depth of 3000 m and terminates at about 3600 m. For G = 20 °C km^{-1}, the corresponding depth range is from 3000 to 4000 m. With decreasing geothermal gradient, the petroleum migration zone extends downwards further. Another point of interest is the temperature changes during the process of kerogen conversion and crack growth. For a geothermal gradient of 40 °C km^{-1}, the temperature change is about 24 °C, which means that the crack growth occurs in the approximate temperature range of 125–150 °C.

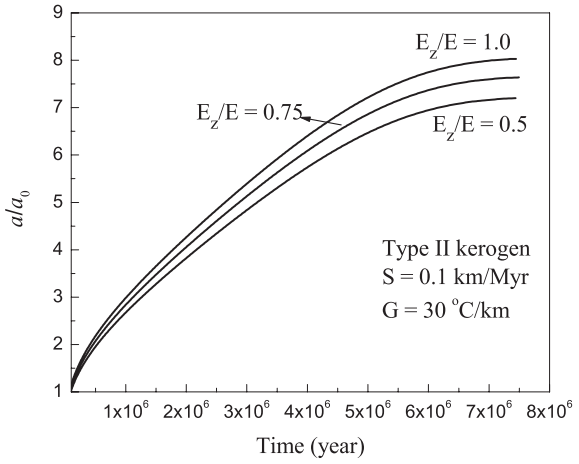

Figure 4. Effect of elastic anisotropy on the crack propagation distance in type II kerogen-bearing source rocks ($S = 0.1$ km Myr^{-1}, $G = 30$ °C km^{-1}).

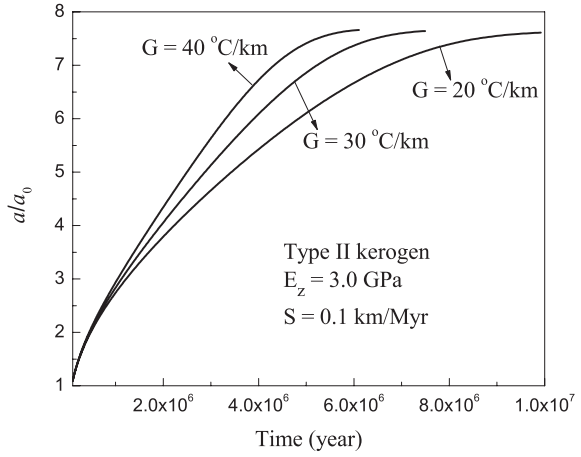

Figure 6. Effect of geothermal gradient on the crack propagation distance in type II kerogen-bearing source rocks ($E_z = 3.0$ GPa, $S = 0.1$ km Myr^{-1}).

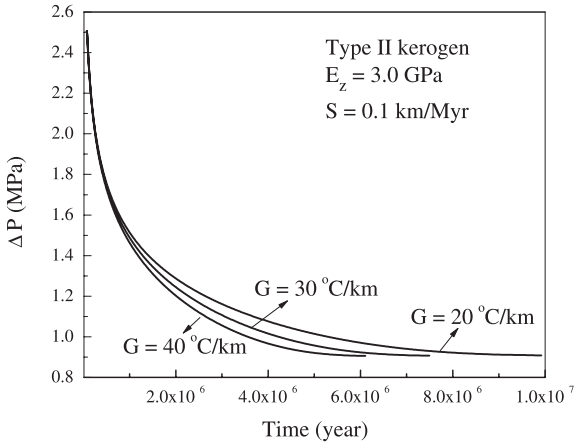

Figure 7. Effect of geothermal gradient on the excess fluid pressure in type II kerogen-bearing source rocks ($E_z = 3.0$ GPa, $S = 0.1$ km Myr^{-1}).

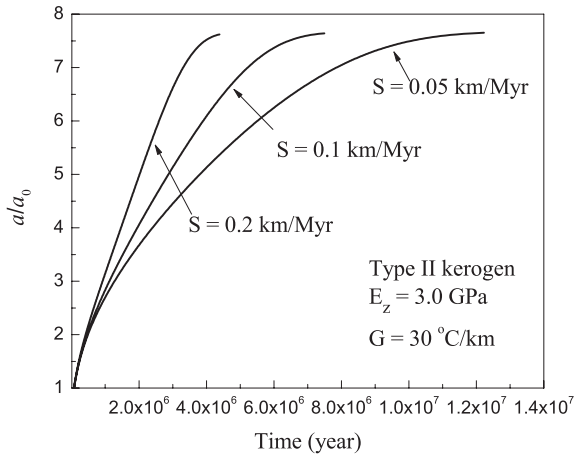

Figure 8. Effect of burial rate on the crack propagation distance in type II kerogen-bearing source rocks ($E_z = 3.0$ GPa, $G = 30$ °C km^{-1}).

For a geothermal gradient of 20 °C km^{-1}, the temperature change is about 20 °C. It is worth noting that although increasing geothermal gradient reduces the duration of crack propagation, it has marginal effect on final crack length and excess pressure.

Figs 8 and 9 show the influence of burial rate on the crack propagation distance and excess pressure, respectively. Variations of crack propagation distance and excess pressure with time for different burial rates follow quite similar patterns to those in Figs 6 and 7, respectively. From eq. (1) the transformation rate of kerogen to petroleum $B\exp[-E_A/R/T(t)]$ increases with increasing burial rate and geothermal gradient. As a result, crack propagation duration reduces significantly at higher burial rate and geothermal gradient. The final crack length and excess pressure, however, are relatively insensitive to the burial rates. In summary, the numerical results in Figs 6–9 show that the geothermal gradient and burial rate have profound influences on the petroleum migration duration but the effect on the final crack length is insignificant.

4 CONCLUDING REMARKS

An integrated approach consisting of fracture mechanics, anisotropic elasticity, kerogen-petroleum transformation kinetics and an equation of state for gas is developed and applied to analyse subcritical propagation of a microcrack filled by oil and gas during

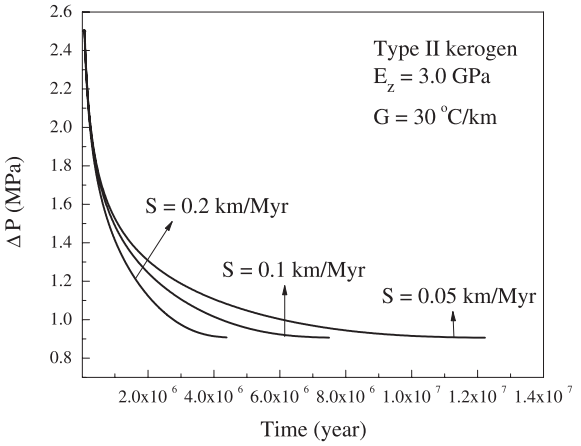

Figure 9. Effect of burial rate on the excess fluid pressure in type II kerogen-bearing source rocks ($E_z = 3.0$ GPa, $G = 30$ °C km^{-1}).

kerogen-petroleum conversion. We focus on the effects of kerogen type and elastic anisotropy of source rock on the crack growth and petroleum migration behaviour. Geothermal gradient and burial rate are included in the theoretical model. The following conclusions can be made based on the numerical results.

(1) Overpressure within well-sealed source rocks resulted principally from conversion of kerogen to petroleum mix can cause microfractures, thus, creating migration pathways for petroleum under favourable burial history.

(2) Microcracks can attain the greatest length in type III kerogen-bearing source rocks due to the higher gas–oil ratio associated with the decomposition of the kerogen. The corresponding crack propagation duration for type III kerogen, however, is longer than those for type I and II kerogen due to the higher activation energy of conversion.

(3) Crack propagation distance becomes shorter in a transversely isotropic source rock with lower modulus ratio E_z/E compared with that in an isotropic rock.

(4) Higher geothermal gradient and fast burial reduce the microcrack propagation duration but only slightly influence the final crack length.

(5) Our simulation results are consistent with the documented field observations that suggest primary migration through self-propagating microfractures may be the most important mechanism for transport of petroleum from low-permeability source layer to higher-permeability carrier layer.

ACKNOWLEDGMENTS

Acknowledgment is made to the Donors of the American Chemical Society Petroleum Research Fund for support of this research (grant number 47463-AC8). We thank two anonymous reviewers for their helpful suggestions. In particular, we would like to thank Professor J. Renner for concrete comments and suggestions on improving upon the presentation of the work.

REFERENCES

Atkinson, B.K., 1984. Subcritical crack growth in geological materials, *J. geophys. Res.,* **89**(B6), 4077–4144.

Berg, R.R. & Gangi, A.F., 1999. Primary migration by oil-generation microfracturing in low-permeability source rocks: application to the Austin Chalk, Texas, *Am. Assoc. Petrol. Geol. Bull.,* **83,** 727–756.

Bredehoeft, J.D., Wesley, J.B. & Fouch, T.D., 1994. Simulations of the origin of the fluid pressure, fracture generation, and the movement of fluids in the Unita basin, Utah, *Am. Assoc. Petrol. Geol. Bull.,* **78,** 1729–1747.

Capuano, R.M., 1993. Evidence of fluid flow in microcracks in geopressured shales, *Am. Assoc. Petrol. Geol. Bull.,* **77,** 1303–1314.

Comer, J.B. & Hinch, H.H., 1987. Recognizing and quantifying expulsion of oil from the Woodford Formation and age-equivalent rocks in Oklahoma and Arkansas, *Am. Assoc. Petrol. Geol. Bull.,* **71,** 844–858.

Duan, Z.H., Moller, N. & Weare, J.N., 1992. An equation of state for the CH_4-CO_2-H_2O system: I. Pure systems from 0 to 1000°C and 0 to 8000 bar, *Geochim. cosmochim. Acta.,* **56,** 2605–2617.

Durand, B., 1988. Understanding of HC migration in sedimentary basins (present state of knowledge), *Org. Geochem.,* **13,** 445–459.

Engelder, T. & Lacazette, A., 1990. Natural hydraulic fracturing, in *Rock Joints,* pp. 35–44, eds Barton, N. & Stephansson, O., A. A. Balkema, Rotterdam.

Fan, Z.Q., Jin, Z.-H. & Johnson, S.E., 2010. Subcritical propagation of an oil-filled penny-shaped crack during kerogen–oil conversion, *Geophys. J. Int.,* **182,** 1141–1147.

Fan, Z.Q., Jin, Z.-H. & Johnson, S.E., 2012. Gas-driven subcritical crack propagation during the conversion of oil to gas, *Petrol. Geosci.,* **18,** 191–199, doi:10.1144/1354-079311-030.

Freiman, S.W., 1984. Effects of chemical environments on slow crack growth in glasses and ceramics, *J. geophys. Res.,* **89**(B6), 4072–4076.

Hunt, J.M., 1979. *Petroleum Geochemistry and Geology,* pp. 69–119, Freeman, San Francisco, CA.

Hunt, J.M., 1990. Generation and migration of petroleum from abnormally pressured fluid compartments, *Am. Assoc. Petrol. Geol. Bull.,* **74,** 1–12.

Jin, Z.-H. & Johnson, S.E., 2008. Primary oil migration through buoyancy-driven multiple fracture propagation: oil velocity and flux, *Geophys. Res. Lett.,* **35,** L09303, doi:10.1029/2008GL033645.

Jin, Z.-H., Johnson, S.E. & Fan, Z.Q., 2010. Subcritical propagation and coalescence of oil-filled cracks: getting the oil out of low-permeability source rocks, *Geophys. Res. Lett.,* **37,** L01305, doi:10.1029/2009GL041576.

Lacazette, A. & Engelder, T., 1992. Fluid-driven cyclic propagation of a joint in the Ithaca silstone, Appalachian Basin, New York, in *Fault Mechanics and Transport Properties of Rocks,* pp. 297–324, eds Evans, B. & Wong, T.-F., Academic Press, London.

Lash, G.G. & Engelder, T., 2005. An analysis of horizontal microcracking during catagenesis: an example from the Catskill delta complex, *Am. Assoc. Petrol. Geol. Bull.,* **89,** 1433–1449.

Law, B.E. & Spencer, C.W., 1998. Abnormal pressure in hydrocarbon environments, in *Abnormal Pressures in Hydrocarbon Environments,* AAPG Memoirs, Vol. 70, pp. 1–11, eds Law, B.E., Ulmishek, G.F. & Slavin, V.I., American Association of Petroleum Geologists, Tulsa, OK.

Lekhnitskii, S., 1968. *Anisotropic Plates,* Routledge Press, London.

Luo, X.R. & Vasseur, G., 1996. Geopressuring mechanism of organic matter cracking: numerical modeling, *Am. Assoc. Petrol. Geol. Bull.,* **80,** 856–874.

Mann, U., 1994. An integrated approach to the study of primary migration, *Geol. Soc. London Spec. Pub.,* **78,** 233–260, doi:10.1144/GSL.SP.1994.078.01.17.

Marquez, X.M. & Mountjoy, E.W., 1996. Microcracks due to overpressure caused by thermal cracking in well-sealed Upper Devonian reservoirs, deep Alberta basin, *Am. Assoc. Petrol. Geol. Bull.,* **80,** 570–588.

Miller, T.W., 1995. New insights on natural hydraulic fractures induced by abnormally high pore pressure, *Am. Assoc. Petrol. Geol. Bull.,* **79,** 1005–1018.

Momper, J.A., 1978. Oil migration limitations suggested by geological and geochemical considerations, *AAPG Course Note Series,* **8,** B1–B60.

Nelson, R.A., 2001. *Geological Analysis of Naturally Fractured Reservoirs,* 2nd edn, Gulf Professional Publishing, Butterworth-Heinmann, Boston, MA.

Nunn, J., 1996. Buoyancy-driven propagation of isolated fluid-filled fractures—implications for fluid transport in gulf of Mexico geopressured sediments, *J. geophys. Res.,* **101,** 2963–2970.

Ozkaya, I., 1988. A simple analysis of oil-induced fracturing in sedimentary rocks, *Mar. Petrol. Geol.,* **5,** 293–297.

Palciauskas, V.V. & Domenico, P.A., 1980. Microfracture development in compacting sediments: relations to hydrocarbon maturation kinetics, *Am. Assoc. Petrol. Geol. Bull.,* **64,** 927–937.

Pepper, A.S. & Corvi, P.J., 1995. Simple kinetic models of petroleum formation. Part I: oil and gas generation from kerogen, *Mar. Petrol. Geol.,* **12,** 291–319.

Tissot, B.P. & Welte, D.H., 1984. Petroleum formation and occurrence, in *A New Approach to Oil and Gas Exploration,* Springer, Berlin.

Tsai, Y.M., 1982. Penny-shaped crack in a transversely isotropic plate of finite thickness, *Int. J. Fract.,* **20,** 81–89.

Vernik, L., 1994. Hydrocarbon generation induced microcracking of source rocks, *Geophysics,* **59,** 555–563.

Vernik, L. & Landis C., 1996. Elastic anisotropy of source rocks: implications for hydrocarbon generation and primary migration, *Am. Assoc. Petrol. Geol. Bull.,* **80,** 531–544.